

MIT Open Access Articles

*The Receptor AXL Diversifies EGFR Signaling
and Limits the Response to EGFR-Targeted
Inhibitors in Triple-Negative Breast Cancer Cells*

The MIT Faculty has made this article openly available. **Please share**
how this access benefits you. Your story matters.

Citation: Meyer, A. S., M. A. Miller, F. B. Gertler, and D. A. Lauffenburger. "The Receptor AXL Diversifies EGFR Signaling and Limits the Response to EGFR-Targeted Inhibitors in Triple-Negative Breast Cancer Cells." *Science Signaling* 6, no. 287 (August 6, 2013): ra66–ra66.

As Published: <http://dx.doi.org/10.1126/scisignal.2004155>

Publisher: American Association for the Advancement of Science (AAAS)

Persistent URL: <http://hdl.handle.net/1721.1/88954>

Version: Author's final manuscript: final author's manuscript post peer review, without publisher's formatting or copy editing

Terms of use: Creative Commons Attribution-Noncommercial-Share Alike



Published in final edited form as:

Sci Signal. ; 6(287): ra66. doi:10.1126/scisignal.2004155.

The Receptor AXL Diversifies EGFR Signaling and Limits the Response to EGFR-Targeted Inhibitors in Triple-Negative Breast Cancer Cells

Aaron S. Meyer^{1,2}, Miles A. Miller¹, Frank B. Gertler^{2,3}, and Douglas A. Lauffenburger^{1,2,3,*}

¹Department of Biological Engineering, Massachusetts Institute of Technology, Cambridge, MA 02139, USA

²David H. Koch Institute for Integrative Cancer Research, Massachusetts Institute of Technology, Cambridge, MA 02139, USA

³Department of Biology, Massachusetts Institute of Technology, Cambridge, MA 02139, USA

Abstract

The relationship between drug resistance, changes in signaling, and emergence of an invasive phenotype is well appreciated, but the underlying mechanisms are not well understood. Using machine learning analysis applied to the Cancer Cell Line Encyclopedia database, we identified expression of *AXL*, the gene that encodes the epithelial-to-mesenchymal transition (EMT)-associated receptor tyrosine kinase (RTK) AXL, as exceptionally predictive of lack of response to ErbB family receptor-targeted inhibitors. Activation of EGFR (epidermal growth factor receptor) transactivated AXL, and this ligand-independent AXL activity diversified EGFR-induced signaling into additional downstream pathways beyond those triggered by EGFR alone. AXL-mediated signaling diversification was required for EGF (epidermal growth factor)-elicited motility responses in AXL-positive TNBC (triple-negative breast cancer) cells. Using cross-linking coimmunoprecipitation assays, we determined that AXL associated with EGFR, other ErbB receptor family members, MET (hepatocyte growth factor receptor), and PDGFR (platelet-derived growth factor receptor) but not IGF1R (insulin-like growth factor 1 receptor) or INSR (insulin receptor). From these AXL interaction data, we predicted AXL-mediated signaling synergy for additional RTKs and validated these predictions in cells. This alternative mechanism

*Corresponding author. lauffen@mit.edu.

SUPPLEMENTARY MATERIALS

www.sciencesignaling.org/cgi/content/full/6/287/ra66/DC1

Fig. S1. Support vector classification to identify mechanisms of drug resistance.

Fig. S2. Single-cell EGFR and AXL expression with R428 treatment.

Fig. S3. RTK crosstalk occurs in TNBC cells.

Fig. S4. Receptor activation is similar in AXL knockdown cells.

Fig. S5. AXL signaling is required for EGF-elicited protrusion.

Fig. S6. A multivariate chemical cross-linking approach to study receptor colocalization.

Fig. S7. Cross-linking can predict receptor transactivation pairs.

Table S1. RTK genes significantly associated with both erlotinib and lapatinib resistance.

Table S2. Single phosphosite or condition analysis provides an incomplete perspective of the signaling effects upon AXL knockdown.

Table S3. Relative model goodness of fits based on the Akaike information criterion.

Author contributions: D.A.L., F.B.G., and A.S.M. conceived the experiments. A.S.M. and M.A.M. performed the experiments and analyzed the data. All authors wrote the manuscript.

Competing interests: The authors declare that they have no competing interests.

Data and materials availability: The CCLE data are freely available (<http://www.broadinstitute.org/ccle/data/browseData?conversationPropagation=begin>). They are used without extensive modification, and the two changes performed (filtering out cell lines with missing data and discretizing cells into resistant or sensitive) are described within the methods.

of receptor activation limits the use of ligand-blocking therapies and indicates against therapy withdrawal after acquired resistance. Further, subadditive interaction between EGFR- and AXL-targeted inhibitors across all AXL-positive TNBC cell lines may indicate that increased abundance of EGFR is principally a means to transactivation-mediated signaling.

INTRODUCTION

Receptor tyrosine kinases (RTKs) are widely abundant and dysregulated in cancers, and have been the focus of targeted therapies for several decades (1). Although inhibitors targeting RTK signaling have shown clinical benefit in certain malignancies, the use of such drugs is unfortunately limited because of primary (innate) or secondary (acquired) resistance that renders therapeutics against seemingly appropriate targets surprisingly ineffective (2). Often, striking initial benefits of such treatments are ultimately futile as a result of quickly developed resistance and disease progression. Recently, activation of alternative RTKs as an important resistance process has been identified (3, 4), although underlying mechanisms are not well understood. Amplification of the targeted signal can also confer resistance, particularly in vivo, where access to the tumor site by therapeutics may be limited (5, 6).

Another process involved in RTK inhibitor resistance is epithelial-to-mesenchymal transition (EMT), a global program that endows epithelial cells with the ability to migrate and invade surrounding tissue (7, 8). In multiple cancers exhibiting initial response to targeted therapeutics, development of secondary resistance correlates with metastatic potential, invasiveness, and mesenchymal-like traits (9–15). Certain transcriptional, posttranscriptional, and posttranslational changes that confer differences in growth factor signaling, migratory capacity, and resistance have been reported (8,16–18). However, the global nature of the EMT program indicates that integrative studies combined with multivariate, systems approaches will be required to elucidate how these diverse changes contribute to disease progression (19).

AXL, the gene that encodes the TAM (TYRO3, AXL, MERTK) RTK family member AXL, is widely overexpressed in cancers and is predictive of poor patient outcome (20–28). Its expression is induced by the EMT program (10, 28–32), and activation of AXL has been linked to resistance to ErbB-targeted therapies (10, 30, 33). Although AXL can be activated by binding its ligand, Gas6, it often appears to be activated in an alternative ligand-independent manner (33–37). Given the prospect for AXL signaling as a potential explanation for EMT-related ineffectiveness of RTK-directed therapeutics, we examined its contribution to RTK-targeted drug resistance and investigated the potential underlying mechanism.

Using machine learning techniques and multivariate signaling network analysis in concert with public databases and our own targeted experiments, we identified *AXL* expression as an exceptionally strong predictor of resistance to ErbB inhibitors. We discovered that triple-negative breast cancer (TNBC) cell lines that had similarly high abundance of both EGFR (epidermal growth factor receptor) and AXL were more sensitive to AXL inhibition than to EGFR inhibition. Resistance of these cell lines to EGFR inhibitors with respect to viability was accompanied by EGFR activation-induced transactivation of AXL in a manner that amplified a subset of downstream signals that are important to invasive motility but are not activated vigorously by EGFR itself. Exploring the mechanism for this resistance-related signaling diversification, we found a correlation between the AXL-mediated lack of response to RTK-targeted drugs and the physical association of AXL with those particular RTKs as characterized by cross-linking coimmunoprecipitation. Indeed, we were able to successfully predict novel AXL transactivation in RTK/ligand pairs by considering

expression and association proclivity. Together, our findings offer new insights concerning RTK signaling crosstalk involving AXL through a transactivation mechanism.

RESULTS

Classification of tumor cell lines identifies AXL as an exceptionally strong predictive marker of resistance to ErbB-targeted drugs

Because activation of alternative receptors is a widespread means of resistance to RTK-targeted inhibitors (3, 4), we used the Cancer Cell Line Encyclopedia (CCLE), a publicly available data set of expression and drug response (38), to examine whether combinatorial expression of multiple RTKs may be related to lack of response to particular RTK-directed drugs. Although straightforward inspection of univariate correlation between expression and drug response is a common approach for hypothesis generation, such an analysis is confounded by broad-ranging expression correlations between genes, particularly genes encoding proteins targeted by the inhibitor. The expression of a single gene may therefore correlate with drug resistance through its correlation with expression of the drug target. Pairwise comparison indicated that RTK expression is either significantly correlated or anticorrelated as often as not (51% of RTK pairs at $P < 0.05$ significance; Fig. 1A and fig. S1A). Therefore, we instead used all possible drug target RTK gene pairs as bivariate predictors in a support vector machine (SVM)-based classification scheme (39) to identify genes whose expression in combination with that of the gene encoding the target RTK synergistically improves prediction of drug response. Briefly, SVM methods aim to find a discriminating threshold based on “inputs” (in this case receptor gene expression) that predict an “output” (in this case sensitivity to drug). By examining whether a set of inputs can discriminate sensitive or resistant cells accurately, we formed hypotheses about whether a particular receptor may play a causal role in drug resistance. As an initial control, the expression of genes encoding the targets of each drug was used on its own to predict sensitivity. To calculate significance for later comparisons, we combined this expression measurement with a random vector, and the distribution of all such trials is shown (blue area, Fig. 1B). This random vector additionally accounts for model performance because of changes in the number of input variables. A more permissive control was created by using solely the random data vectors in repeated trials (black area, Fig. 1B). Completely randomized data did not necessarily predict half of the cell lines correctly, as a result of asymmetry in the number of cell lines in each class (resistant or sensitive). Not surprisingly, expression of the gene that encodes the inhibitor-targeted RTK was always among the strongest independent predictors of drug response and was significantly more predictive than only random inputs.

Given that drug sensitivity can be reduced by redundancy among RTKs, we tested whether a model that considered the expression of the gene encoding the targeted RTK along with the expression of a gene encoding another RTK was better at predicting drug response than the model considering the drug target RTK alone. The predicted response to the ErbB-targeted drugs lapatinib and erlotinib was significantly improved by considering AXL expression, whereas the prediction of response to the IGF1R (insulin-like growth factor 1 receptor)-targeted drug AEW541 was not substantially improved (Fig. 1B). The expression of genes that encode TAM ligands (such as Gas6 and protein S) or other TAM receptors (TYRO3, MERTK) all failed to generate synergistic prediction improvement when combined with that of the drug target RTK alone, with that of AXL, or with that of the drug target RTK and AXL (fig. S1B). With respect to directionality, the classifier for sensitivity to the EGFR inhibitor erlotinib using AXL and EGFR expression (fig. S1C) yielded the prediction that EGFR expression indicates increased sensitivity, whereas AXL expression indicates increased resistance (Fig. 1C). In contrast, univariate analysis predicted no relationship

between *AXL* expression and erlotinib sensitivity (Fig. 1D). Methods depending only on *AXL* expression likely do not capture a relationship because *AXL* and *EGFR* are themselves correlated in expression ($P < 10^{-32}$, Spearman correlation, from the CCLE), convoluting simpler analyses as we argued above. This correlation additionally exists within clinical tumors ($P < 10^{-17}$, Spearman correlation, from the CCLE); however, our aim is not to ascribe significance to correlation between the two receptors but rather to point out this convoluting factor in univariate analyses (40). Our modeling therefore identified *AXL* expression as a common marker for resistance to ErbB-targeted but not IGFR-targeted therapies. Inhibitors that target MET [hepatocyte growth factor (HGF) receptor] and PDGFR (platelet-derived growth factor receptor), for which sensitivity data are available, target multiple receptor families; therefore, a meaningful analysis could not be readily performed. Although *AXL* expression showed the highest significance in this analysis, that of *EPHA1* and *FGFR1* also exhibited similarly high significance (table S1). Expression of these genes has been implicated similarly in resistance to ErbB-targeted therapies in breast carcinoma (3, 41).

Although *AXL* has been shown previously to confer secondary resistance to lapatinib and erlotinib in other cancer subtypes, including HER2 (human epidermal growth factor receptor 2)-positive breast cancer and non-small cell lung cancers (30, 33), we focused on a role for *AXL* in modulating the response of TNBC cells to EGFR-targeted drugs. Despite high abundance and activation of EGFR in TNBC, EGFR inhibitors have not been efficacious on their own, so discerning explanations for the lack of sensitivity could be important both for understanding basic aspects of EGFR signaling and for potentially improving therapeutic strategies. Because TNBC cell lines typically express both *EGFR* and *AXL* endogenously, our model would indeed predict *AXL*-related resistance to erlotinib in these cells. Extrapolating from the observation that inclusion of *AXL* expression improved the predictive capacity of the model, we additionally reasoned that simultaneous inhibition of *AXL* and EGFR would result in synergistic cytotoxicity in TNBC and that these cells would be more sensitive to *AXL* inhibitors than to EGFR inhibitors. We treated three such cell lines with erlotinib and R428, a specific inhibitor of *AXL*, and confirmed that they are resistant to EGFR inhibition and sensitive to *AXL* inhibition (Fig. 1E). Additionally, treatment with R428, but not erlotinib, showed synergistic cytotoxicity with paclitaxel in a subset of cells (fig. S1, D and E), consistent with previously reported findings that targeted RTK inhibition can operate synergistically with DNA-damaging agents (42, 43). However, we were surprised to observe a subadditive interaction between the EGFR- and the *AXL*-targeted inhibitors in dually treated cells (Fig. 1E). Although these results validate the prediction of erlotinib resistance in these cells, validation of *AXL* as the mechanism of resistance would typically be expected to show synergy in the combined effects of erlotinib and R428. Because subadditive interactions can indicate shared pathway components, we wondered whether inhibition of one receptor might decrease the activity of the other. A second possibility, in which two distinct cell populations exist—one in which both *AXL* and *EGFR* are expressed and is sensitive to both drugs, and another in which neither is expressed and is resistant to both drugs—would similarly explain our observations but not constitute drug antagonism. However, single-cell analysis revealed neither distinct populations of cells nor changes in receptor expression upon drug treatment (fig. S2).

AXL knockdown impairs EGFR signaling

To test our model, we probed whether *AXL* and other RTKs outside the ErbB family are activated upon EGF (epidermal growth factor) stimulation. Using MDA-MB-231 cells, we measured pan-phosphotyrosine abundance on immunoprecipitated receptors and found that MET and *AXL* were phosphorylated after cells were treated with EGF (Fig. 2A). In contrast, we did not observe phosphorylation of EGFR upon activation of *AXL* with an activating

antibody, demonstrating that, although activation of EGFR can induce the transactivation of AXL, the reverse does not transpire (fig. S3A).

Because the expression of *AXL*, but not that of the gene encoding its ligand Gas6, predicted resistance to ErbB inhibitors (fig. S1B) and because previous studies have verified Gas6-independent resistance effects of AXL signaling (33), we hypothesized that AXL may also modulate signaling responses elicited by activation of other RTKs. To test this, we transfected MDA-MB-231 cells with an siRNA (small interfering RNA) pool targeting AXL (Fig. 2B) and then stimulated cells with EGF, TGF α (transforming growth factor- α), or HGF and measured the phosphorylation of 11 downstream phosphosites. The surface and total (Fig. 2C) abundance of other receptors were unchanged by AXL knockdown, and the phosphorylated (fig. S3B) abundance was unchanged by treatment with R428. However, nearly all downstream phosphosites were affected by AXL knockdown, either in control or in growth factor-stimulated cells (Fig. 2D and table S2), indicating that AXL-dependent signaling effects may be global in nature and emphasizing the importance of multivariate analysis because of the limited use of focusing on a single signaling pathway. Similar effects on the phosphorylation of two proteins were observed in cells treated with the AXL-specific inhibitor R428 (fig. S3C), indicating that these effects depend on the kinase activity of AXL. Western blotting for a subset of phosphosites quantitatively matched our ELISA (enzyme-linked immunosorbent assay) measurements (fig. S3D). Attempting to directly stimulate AXL with Gas6 did not elicit a substantial signaling response, and these signaling consequences were small compared with EGF-elicited, AXL-dependent signaling effects (fig. S3E). This observation is similar to results in other studies of Gas6-elicited signaling in MDA-MB-231 (44). Why different cell lines display markedly distinct receptor activation patterns to Gas6 remains a question for future studies (44–46).

To investigate the crosstalk between AXL and EGFR (as well as MET) signaling further, we next examined the ratio of fold activation (phosphorylation) of various signaling proteins in the absence versus presence of AXL (Fig. 3A). The unstimulated conditions represented signaling network activity presumably arising from constitutive autocrine processes. This analysis revealed more widespread AXL-dependent effects in EGF- or TGF α -stimulated cells compared with HGF-stimulated cells, with the largest difference in activation observed for GSK3 (glycogen synthase kinase 3) and Akt. Further, the relative magnitude of effects across the phosphosites investigated was correlated between EGF- or TGF α -stimulated cells and unstimulated cells but was not correlated between HGF-stimulated and unstimulated cells (Fig. 3A, inset). These results suggest that AXL may mediate similar basal and EGFR-stimulated signaling pathways in TNBC cells, whereas HGF yields a distinct downstream AXL-mediated signature.

We then performed principal components analysis (PCA) to gain insight concerning the network-level variation in signaling across these treatment conditions (Fig. 3B). Principal component 1 (PC1) was found to correspond to EGF-induced signaling, and PC2 to HGF-elicited signaling, with TGF α having an intermediate effect. Knockdown of AXL moved cells negatively along PC1 and reduced the magnitude of the effect of EGF stimulation. Examination of the loading plot revealed separation between phosphosites only mildly affected by knockdown [for example, phosphorylation of STAT3 (signal transducer and activator of transcription 3) and JNK (c-Jun N-terminal kinase)] and those strongly affected (such as the phosphorylation of Akt and GSK3), with the rest scattered at intermediate locations (Fig. 3C). Together, these data indicate that EGF and TGF α induce ErbB-mediated downstream signaling that is qualitatively similar to basal signaling but is distinct from MET-mediated signaling, and this baseline-like signaling is disrupted by AXL knockdown. The difference between HGF and EGF, TGF α , and baseline signaling is likely a result of the absence of signaling from EGFR, HER2, or AXL in the former case, because MET is

presumably transactivated also in the EGF- or TGF α -stimulated cases. An appealing interpretation is that autocrine EGFR ligand activity is constitutive and transactivates AXL.

AXL amplifies signaling in the EGFR-associated pathway but does not sensitize EGFR to its ligand

Because receptor activation can be quantitatively characterized in terms of ligand concentration-related sensitivity and maximal activation at saturation, we investigated how AXL influences the dose response of EGFR to EGF. We stimulated MDA-MB-231 cells with a range of concentrations of EGF and measured the pan-phosphotyrosine on EGFR and the phosphorylation of Akt (Fig. 4, A and B). Phosphorylation of Akt was chosen for measurement as a critical downstream signal that was strongly influenced by AXL knockdown, though not to imply that all transactivation-mediated effects are regulated through Akt alone (Fig. 3C). Phosphorylation of EGFR was unaffected by AXL knockdown except at very high (above saturating) EGF concentrations (Fig. 4A), likely as a result of altered trafficking or cellular processes induced at such nonphysiological amounts of stimulation. Other receptor-proximal components, such as the adaptor protein SHC and the CDC2 kinase, exhibited similar phosphorylation after stimulation at the EGF dose used in the signaling studies here (fig. S4). In contrast, AXL knockdown affected the phosphorylation of Akt in response to all doses of EGF by a shift in magnitude (“vertically”) rather than in sensitivity (“horizontally”) (Fig. 4B). To deconvolve these concomitant changes in the phosphorylation of EGFR and Akt, we plotted the abundance of phosphorylated Akt as a function of phosphorylated EGFR in cells treated with either control siRNA or AXL siRNA (Fig. 4C). This revealed a uniform downward shift across all stimulation amounts in the absence of AXL, indicating a consistent fold change in the magnitude of signal transduction. Each curve could be well described to first approximation by a Hill function, with comparable K_d (threshold of half-maximal activation) but markedly different maximal activation (Fig. 4D). To identify the level at which this regulation may occur, we fit these data to alternative models of signal transduction from the receptor layer (see Materials and Methods). The data were best explained by a model in which basal and stimulated AXL activities exist, the latter in proportion to EGFR activation and in which transduction of both signals occurs through separately saturable processes (table S3). This model is consistent with our biochemical observations (Fig. 2A). The effect of baseline activation of AXL can be observed from the plot of phosphorylated Akt as a function of pan-phosphotyrosine EGFR, where at low EGFR activation in the presence of AXL, the phosphorylation of Akt was higher than a simple Hill regression would suggest (Fig. 4C). Biologically, this indicates that the components downstream of the receptor are saturated by maximal EGFR activation and that, at least with respect to phosphorylated Akt, the transactivation of AXL increases the effective amount of RTK signaling and amplifies the signaling consequence of stimulation.

Multipathway signaling correctly predicts AXL knockdown inhibition of EGF-stimulated protrusion

We next asked how the broad effects on signaling that resulted from AXL knockdown might influence the migration behavior of cells. We elected to use acute membrane protrusion as a surrogate measurement of three-dimensional migratory capacity on the basis of our previous findings that this assay corresponds well to growth factor-stimulated invasive motility within extracellular matrix (47). Protrusion measurements from wild-type MDA-MB-231 cells were used to train a family of partial least-squares regression models for how protrusion activity depends on multiple phospho-proteomic signals. Minimal models that use only three signals were examined to ascertain the most vital pathway predictors for growth factor-induced motility. We identified models that fit the data by cross-validation ($Q_2 > 0.6$) and found that these were enriched in inclusion of GSK3, STAT3, and Akt as the key

predictor signals (fig. S5A). These models involved similar weights for the predictor signals in both PCs, demonstrating consistency across the ensemble of top-fitting models in their multipathway signaling-to-protrusion relationships (Fig. 5A).

This ensemble of models was then used to predict wild-type MDA-MB-231 protrusion by cross-validation and to a priori predict protrusion modulation by AXL knockdown (Fig. 5B). EGF-stimulated protrusion was predicted to be the most substantially attenuated response after AXL knockdown, whereas HGF-stimulated protrusion was predicted to remain essentially unaffected. These predictions were indeed correct in MDA-MB-231 cells transfected with AXL siRNA: HGF-elicited protrusion was not significantly affected, whereas EGF-elicited protrusion was significantly reduced (Fig. 5C). Treatment with R428 confirmed that EGF-stimulated protrusion depended on AXL-mediated signaling in another TNBC line, MDA-MB-157, but that it did not in two other breast cancer cell lines, MCF7 and T47D, which lack AXL expression (Fig. 5D). The effect of R428 phenocopied that of AXL siRNA treatment in terms of the protrusion response to EGF in MDA-MB-231 cells (Fig. 5, C and D). TGF α -stimulated protrusion was also reduced in MDA-MB-231 cells by R428 treatment, although to a lesser degree, which was in accord with our model predictions (fig. S5B). These results indicate that along with amplification of EGFR-induced downstream signaling, the transactivation of AXL additionally activates a qualitatively distinct set of signals that are important for cell migration in response to stimuli. Moreover, our three-pathway partial least-squares regression model successfully captured the integrated effects of these signals on this phenotypic response.

AXL is in proximity to ErbB and MET but not IGF1R or IR

We investigated whether the transactivation of AXL (and MET) by EGFR might involve physicochemical proximity of these RTKs. Because of technical limitations in capability for distinguishing receptor colocalization by other methods (fig. S6, A and B), we used a technique in which immuno-precipitation of cross-linked receptors from lysate was performed in a multiplexed fashion on barcoded fluorescent beads. The degree of AXL cross-linking with each of various other RTKs was quantified using an AXL antibody (Fig. 6A). Across multiple cell lines, we observed a significant degree of AXL cross-linking with ErbB receptors, MET, and PDGFR but not with insulin receptor (INSR) or IGF1R (Fig. 6B and fig. S6C). The amount of AXL cross-linking was roughly proportional to the abundance of that particular RTK—with the exception of INSR and IGF1R, neither of which garnered cross-linked AXL to a measureable extent (Fig. 6C). We confirmed cross-linking results with reciprocal immunoprecipitation assays in MDA-MB-231, in which we observed the association of AXL with EGFR but not with IGF1R (fig. S6D).

On the basis of these data, we sought a quantitative framework to understand the respective amounts of complexing observed between AXL and each RTK across different cell lines. According to fundamental stoichiometric considerations, the amount of AXL observed in complex with a particular RTK in a particular cell line should be approximately the product of the RTK abundance in that cell line, with proportionality described by coefficients constituting (i) the cross-linking and protein loading efficiency and (ii) the antibody immunoprecipitation efficiencies and extent of colocalization. With measurements of RTK abundance and the amount cross-linked to AXL, we determined the remaining parameters (see Materials and Methods) to provide a way to account for differences in receptor expression when interpreting cross-linking data (fig. S6D). With this quantitative formulation, we could then calculate whether the parameter characterizing AXL/RTK colocalization deviated significantly from 0 for each RTK (Fig. 6D). Significant deviation from 0 indicates colocalization. Despite IGF1R and INSR being substantively abundant in various cell lines, the calculated likelihood that they localized with AXL was not significant.

Although this parameter includes the efficiency of immunoprecipitating IGF1R or INSR, we verified that these two receptors were detected with similar efficiency both by direct ELISA of the same cell lysates and by quantification of a recombinant standard. We additionally confirmed cross-linked immunoprecipitation between AXL and EGFR to the exclusion of IGF1R by reciprocal immunoprecipitation in MDA-MB-231 (fig. S6E). Our quantitative analysis framework ruled out the possibility that merely low abundance of IGF1R and INSR was a trivial explanation for the absence of significant colocalization. We therefore conclude that AXL is colocalized with ErbB, MET, and PDGFR but not with IGF1R or INSR.

The amount of EGFR-AXL complex was much greater in MDA-MB-231 than in other cell lines, likely as a result of the differences in abundance of EGFR (Fig. 6C). MCF7 cells transfected with AXL and treated with EGF showed no synergistic response characteristic of receptor transactivation, consistent with the relatively little EGF-elicited signaling overall (fig. S7A). We therefore considered whether we could predict the importance of AXL transactivation induced by activation of RTKs other than EGFR. MDA-MB-453 cells have large amounts of HER2 and HER3 in complex with AXL, so our notion would predict that AXL signaling might contribute to a heregulin (HRG)-stimulated response in these cells. We learned by direct test, using AXL transfection and HRG treatment, that this is in fact observed (Fig. 7A and fig. S7B). We analogously predicted that the relative degree of synergistic HRG-induced signaling should be similar to the difference in signaling between EGF, TGF α , HGF, HRG, HBEGF (heparin-binding EGF-like growth factor), and IGF, if the effect of clustering can be resolved from single RTK-specific effects. That is, phosphorylation sites that show synergistic activation should be relatively less stimulated by IGF stimulation because IGF1R does not display comparable AXL colocalization. Indeed, the magnitude of synergy induced by HRG and AXL signaling correlated significantly with colocalized RTK-specific signaling (Fig. 7B and fig. S7C). This indicates that RTK/AXL colocalization can predict RTK-mediated AXL transactivation and that this transactivation leads to similar downstream signaling not obtained through activation of IGF1R or INSR.

DISCUSSION

Differential expression between two sets of cells or tumors is often used as evidence for the functional significance of particular genes but ignores the intricate correlation present between genes that can lead to spurious associations in targeted studies. We interrogated a large publicly available data set derived from cancer cell lines to examine the role of receptor expression in resistance to RTK-targeted therapeutics and found that *AXL* expression synergizes with expression of the gene encoding the targeted receptor when predicting resistance to erlotinib and lapatinib. However, as a result of co-expression of *AXL* and *EGFR*, this relationship could not be clearly identified by univariate analyses. Although activation of AXL has been implicated in resistance to ErbB inhibitors in both lung cancer and HER2-positive breast cancer (30, 33), our analysis suggests that *AXL* expression may be a common marker of EGFR inhibitor resistance in TNBC and possibly in other subtypes of breast carcinoma (Fig. 1B). Using dedicated experimental tumor cell cultures, we discovered a synergistic interaction between ErbB and AXL signaling in which AXL transactivation mediated by associated EGFR amplified the response of a subset of downstream elements, quantitatively shifting emphasis of the downstream network across multiple pathways. This diversification contributed in a critical manner to the migration and efficient proliferation of TNBC cells in response to EGF (Figs. 1E and 5D). Moreover, we found that this transactivation appeared to result from physical clustering interactions, which are quantitatively restricted to certain RTKs depending on a combination of intrinsic “affinity” and expression (Fig. 6, C and D). We also predicted additional RTK/ligand contexts in which AXL synergistically amplified downstream signaling (Fig. 7).

Context-dependent physical interaction between EGFR and AXL has recently been appreciated (48). Our data indicate that ErbB, MET, and AXL receptors exist in local clusters on the plasma membrane, though do not distinguish between distinctly bound complexes and diffusional proximity. Because IGF1R and INSR are the only receptors examined here not found in complex with AXL, and IGF1R seems to be qualitatively distinct in its inability to provide compensatory resistance, we expect that this clustering may be important to the signaling that confers resistance (3). Clustering may arise as a consequence of mutual interactions with the extracellular matrix, weak lipid interactions, or shared scaffold interactions. Our observations along with previous reports are consistent with the phenomenon that clustering leads to subsequent activation-dependent enhancement of interactions after stimulation (48), with striking correlation between the receptors that are activated in trans and their localization on the cell surface (37). Future work is needed to perturb this clustering specifically and examine the extent to which such clustering is required for resistance, trans-activation, and diversification of receptor signaling. If clustering is required for these effects, drugs targeting the interaction mechanism may be efficacious in counteracting this signal diversification, thereby bolstering RTK-targeted therapy effectiveness.

These results carry clinical significance in the design of therapies targeting AXL and MET signaling, particularly within TNBC. Subadditive cytotoxicity after dual treatment with AXL and EGFR inhibitors suggests that the TNBC cells investigated here may be more reliant on AXL or MET for downstream signaling than EGFR itself, and that the effects of increased EGFR abundance may be in large part manifested by activation of AXL or MET. If dispensable for survival, EGFR is still important for directing metastatic dissemination, and our results suggest that transactivation may be important for promoting such an invasive response (49). Activation by alternative receptors indicates that treatments blocking ligand binding to AXL and MET, an area of active investigation (50–53), may not be effective in blocking signaling from these receptors, and that inhibitors of their kinase activity or treatments that reduce receptor abundance may be more effective (51, 54). Transactivation-mediated signaling may additionally be a means of secondary resistance to MET or AXL ligand-blocking treatments. In other carcinomas, EMT and the expression of AXL and *c-MET* have been identified as a mechanism of secondary resistance to ErbB-targeted therapies (30, 33). Crosstalk in these cells, particularly after ErbB-targeted treatment, is halted because of RTK-mediated secondary resistance and may provide qualitatively distinct signaling through new receptors, though in response to the original activating ligand. Consequently, upon withdrawal of treatment, cells could respond to the original ligand with a more invasive or aggressive phenotype as a result of the dynamic network rewiring that created resistance (55–57). Finally, given the striking similarities in signaling and resistance profiles of AXL and MET, as well as the observation that MET can drive AXL expression (58), inhibition of both receptors simultaneously in drug design may be desirable.

Our work more broadly raises the implication that modulation of RTK expression may not simply dictate response to stimulation by a receptor's cognate ligand, but that particular receptor pairs can communicate in a directional manner. Thus, cancer therapies targeting ligand interaction may be circumvented by activation in trans, and quantitative changes in inhibitor resistance may take place by amplification of signaling through other receptors. Future work is needed to gauge the extent and exact molecular mechanism of interfamily transactivation, the mechanisms of preclustering, as well as the exact signals that are sufficient for therapeutic resistance through activation of alternative receptors.

MATERIALS AND METHODS

Antibody reagents, growth factors, and inhibitors

EGF, PDGF-BB, and TGF α were purchased from Invitrogen. HGF, IGF1, HBEGF, and HRG were purchased from PeproTech. Unless otherwise indicated, EGF and Gas6 (R&D Systems) were used at 100 ng/ml. TGF α , PDGF-BB, HBEGF, and HGF were used at 50 ng/ml. HRG was used at 80 ng/ml. AF154 (R&D Systems) was used at 900 ng/ml. Biotinylated AXL detection, capture, and activating antibodies were purchased from R&D Systems. EGFR, GAPDH (glyceraldehyde-3-phosphate dehydrogenase), EGFR pTyr¹¹⁷³, EGFR pTyr¹⁰⁶⁸, EGFR pTyr¹⁰⁴⁵, SHC pTyr³¹⁷, Cdc2 pTyr¹⁵, ERK (extracellular signal-regulated kinase) pThr²⁰²/pTyr²⁰⁴, Akt pS⁴⁷³, and α -actinin were used for Western blotting and purchased from Cell Signaling Technology. AXL (Santa Cruz Biotechnology) and Cav1 pTyr¹⁴ (Sigma) were also used for Western blotting.

R428 was purchased from Synkinase. AXL SMARTpool ON-TARGETplus siRNA, nontargeting SMARTpool ON-TARGETplus siRNA, and DharmaFECT 4 were purchased from Thermo Scientific. Lipofectamine 2000 was purchased from Invitrogen.

ELISA-based signaling measurements were performed according to the manufacturer's instructions (Bio-Rad). In all cases, pERK is ERK1/2 (pThr¹⁸⁵/pTyr¹⁸⁷, pThr²⁰²/pTyr²⁰⁴), pGSK3 is GSK3 α/β pSer²¹/pSer⁹, pJNK is JNK pThr¹⁸³/pTyr¹⁸⁵, pP38 is P38 pThr¹⁸⁰/pTyr¹⁸², pcJun is c-Jun pSer⁶³, pHSP27 is HSP27 pSer⁷⁸, pIRS1 is IRS1 pSer⁶³⁶/pSer⁶³⁹, pSrc is Src pTyr⁴¹⁶, pSTAT3 is STAT3 pTyr⁷⁰⁵, pTyk2 is Tyk2 pTyr¹⁰⁵⁴/pTyr¹⁰⁵⁵, and pAkt is Akt pSer⁴⁷³.

Lysis was performed with 50 mM tris-HCl (pH 7.5), 10% glycerol, 150 mM NaCl, and 1% NP-40, with complete protease (Roche) and phosphatase (Boston BioProducts) inhibitors added before use.

Cell culture

MDA-MB-231, MDA-MB-157, T47D, MDA-MB-453, SKBR3, and MCF7 cells were cultured in high-glucose Dulbecco's modified Eagle's medium (DMEM) supplemented with 10% fetal bovine serum (FBS) and 1% penicillin-streptomycin. For knockdown, 5×10^5 MDA-MB-231 cells in a 10-cm plate were transfected with 125 pmol of nontargeting siRNA or siRNA targeting AXL using DharmaFECT 4 according to the manufacturer's instructions. All further analysis was performed 48 hours after siRNA transfection. For AXL overexpression, untagged AXL in pIRESpuro2 was transfected with Lipofectamine according to the manufacturer's instructions, and further experiments were performed 12 hours later.

Signaling analysis

Cells were seeded sparsely in six-well plates overnight and serum-starved for 4 hours in DMEM with 0.35% bovine serum albumin and 1% penicillin-streptomycin. After starvation, cells were stimulated with EGF, TGF α , or HGF for 5 min and lysed. Protein concentration was measured with BCA (bicinchoninic acid) assay. When used, inhibitors were added upon serum starvation.

Protrusion measurement

Glass-bottomed dishes (MatTek) were coated with 0.2% Matrigel in serum-free medium for 30 min. Cells were seeded sparsely overnight and serum-starved for 4 hours in L15 medium with 0.35% bovine serum albumin. Inhibitors, when indicated, were added at the beginning of serum starvation and present in the stimulatory bolus. Differential interference contrast

images were acquired every 10 s for 1 min before stimulation and 9 min after stimulation. Cell areas were traced immediately before stimulation and 9 min after stimulation with ImageJ (National Institutes of Health). Single-cell information was aggregated from at least three independent experiments.

Receptor cross-linking

For MDA-MB-231, 5×10^5 cells in 10-cm dishes were transfected with either siRNA targeting AXL or a nontargeting control, and the next day, the cells were plated at identical densities. Two days after transfection, cells were starved for 4 hours and cross-linked using 1 mM EGS for 30 min at 4°C. For MCF7, SKBR3, T47D, and MDA-MB-453, 50% confluent 15-cm plates were transfected with 20 mg of AXL in the IRESpuro2 vector. The next day, cells were starved for 4 hours and cross-linked using 1 mM EGS for 30 min at 4°C. Cells were lysed and normalized by total protein. Measurement of cross-linking was performed by modification of a kit for total RTK measurement (Novagen). Briefly, lysates were diluted twofold in assay buffer and incubated with capture beads for RTKs other than AXL overnight. The lysates were then cleared, and the beads were washed with wash buffer and then incubated with a biotinylated antibody for AXL for 1 hour. After washing again, the beads were incubated with streptavidin-conjugated phycoerythrin for 30 min and then quantified with a Bio-Plex 200 (Bio-Rad Laboratories).

Support vector classification

All numerical analysis was performed within MatLab (MathWorks). Cell lines were classified according to their published drug response, measured as cell viability with CellTiter-Glo after 72 hours, and expression (38). Microarray expression measurements were processed by the robust multiarray average method as described in the original publication. A cell line was considered resistant to the selected drug if its IC_{50} (median inhibitory concentration) was reported to be greater than 8 μ M. This cutoff was selected somewhat arbitrarily because it was the maximum dose tested; however, other cutoffs produced identical results. This method of classification largely agreed with classification based on activity areas and EC_{50} (median effective concentration) values. Cell lines without corresponding drug and expression measurements were thrown out.

As an initial control (blue region, Fig. 1B), the targets of each drug were used on their own to predict sensitivity. The drug target was always among the strongest independent predictors of drug response. To calculate significance for later comparisons, this expression measurement was combined with a pseudorandom vector generated with the *randn* function, and the process was repeated 10^4 to 10^8 times depending on the significance stringency being tested.

Another control (black region, Fig. 1B) was created by using only the random data vector in repeated trials. Prediction with the drug target was always significantly higher than with only random data. Thus, with these controls, expression of another RTK was considered to be predictive of drug sensitivity if a model of the RTK with the drug target was above the 95th quantile of the blue and black lines.

Classification was performed with the *svmtrain* function in MatLab using a linear kernel and quadratic programming optimization method. A quadratic kernel or other optimization methods led to qualitatively identical results. The probes corresponding to AXL and EGFR expression were 558_at and 1956_at, respectively.

Synergy significance

The Loewe interaction model was used to evaluate synergy or antagonism (59):

$$1 = \frac{D_1}{IC_{50,1} \left(\frac{E}{E_{con} - E} \right)^{\frac{1}{m_1}}} + \frac{D_2}{IC_{50,2} \left(\frac{E}{E_{con} - E} \right)^{\frac{1}{m_2}}} + \frac{\alpha D_1 D_2}{IC_{50,1} IC_{50,2} \left(\frac{E}{E_{\infty} - E} \right)^{\frac{1}{2m_1} + \frac{1}{2m_2}}}$$

where D_1 and D_2 are the concentrations of the first and second drugs, respectively; $IC_{50,1}$ and $IC_{50,2}$ are the IC_{50} values of each drug; and m_1 and m_2 are a shape parameter for each drug. E_{con} is the viability of untreated cells, and E is the viability of cells for the respective drug concentrations. Viability data were normalized such that the maximum measurement was scaled to 1, and E_{con} was set to be 1. Last, α is the Loewe synergy parameter, which is negative for antagonism, positive for synergy, and zero for additive effects. Because of the lack of analytical expression for E , the value of E was calculated with *lsqnonlin* by solving for the value that minimizes:

$$\arg \min_{E \in [0,1]} \left| \frac{D_1}{IC_{50,1} \left(\frac{E}{1-E} \right)^{\frac{1}{m_1}}} + \frac{D_2}{IC_{50,2} \left(\frac{E}{1-E} \right)^{\frac{1}{m_2}}} + \frac{\alpha D_1 D_2}{IC_{50,1} IC_{50,2} \left(\frac{E}{1-E} \right)^{\frac{1}{2m_1} + \frac{1}{2m_2}}} - 1 \right|$$

Fitting was performed with the *nlinfit* function within MatLab with initial parameters identified by inspection of the single drug data. Optimization was unconstrained but IC_{50} values were in all cases significantly positive, and all m values were significantly negative as verification of effective fitting. Confidence intervals presented were calculated from the empirically derived Jacobian with the *nlparci* function. Significance was separately verified by jackknife (60).

Partial least-squares regression and PCA

Replicate measurements were averaged and each signaling variable was mean-centered and variance-normalized before further analysis. PCA was performed with singular value decomposition within the *pca* function. The first two components explained 83% of the variance.

For reduced partial least-squares modeling, the output variable was assembled from mean protrusion measurements for each growth factor, and the unstimulated condition set to 0. Model reduction was performed by training models with all possible combinations of three input variable sets. Three variables were chosen, as it was the smallest model size with sufficient well-trained models to ensure robust variable enrichment. Model reduction with larger reduced models produced qualitatively similar results. Each individual reduced model was then used concomitantly, and the results were shown by displaying the average and SE of loading values and predictions. As a result of variation in baseline signaling, predictions for knockdown cells were taken to be the prediction for the knockdown and stimulated condition minus the prediction of the knockdown and unstimulated condition.

Amplification modeling

Each model was fit with the *nlinfit* function. To ensure robustness with respect to initial parameter selection, fitting was performed 100 times with randomly selected initial parameters within the range of feasible values. ξ is 0 with AXL knocked down and 1 with AXL present. [pEGFR] and [pAkt] are from measurements of pan-phosphotyrosine EGFR and pAkt across a dose range of EGF. Models were compared using the corrected and uncorrected Akaike information criterion denoted AICc and AIC, respectively (61).

To fit data to a model in which activation of AXL is in proportion to EGFR activation, and signaling integration is receptor-proximal, Eq. 1 was used:

$$[pAkt] = \frac{B_{\max}([pEGFR] + \alpha [pEGFR] \xi)}{K_D + ([pEGFR] + \alpha [pEGFR] \xi)} + B_0$$

For a model in which amplification of Akt activation with respect to a set amount of EGFR activity, and AXL only affects this proportional relationship, Eq. 2 was used:

$$[pAkt] = \frac{B_{\max}(1 + \alpha \xi) [pEGFR]}{K_D + [pEGFR]} + B_0$$

For a model in which no signaling effect from AXL exists, Eq. 3 was used:

$$[pAkt] = \frac{B_{\max} [pEGFR]}{K_D + [pEGFR]} + B_0$$

For a model in which some baseline activation of AXL is possible in addition to proportional activation, and signaling integration is receptor-proximal, Eq. 4 was used:

$$[pAkt] = \frac{B_{\max}([pEGFR] + \alpha [pEGFR] \xi + \xi \beta)}{k_D + ([pEGFR] \alpha [pEGFR] \xi + \xi \beta)} + B_0$$

For a model in which Akt activated by AXL and activated by EGFR is summed with proportional activation of AXL, Eq. 5 was used:

$$[pAkt] = \frac{B_{\max,1} [pEGFR]}{k_{D,1} + [pEGFR]} + \frac{\xi B_{\max,2} [pEGFR]}{K_{D,2} + [pEGFR]} + B_0$$

For a model in which no signaling effect from AXL through EGFR pathway exists, but there is a baseline effect of AXL present, Eq. 6 was used:

$$[pAkt] = \frac{B_{\max} [pEGFR]}{k_D + [pEGFR]} + \xi \beta + B_0$$

For a model with only baseline activation of AXL, and signaling integration is receptor-proximal, Eq. 7 was used:

$$[pAkt] = \frac{B_{\max} [pEGFR] + \alpha \xi}{k_D + [pEGFR] + \alpha \xi} + B_0$$

For a model with Akt activated by AXL and activated by EGFR summed, with proportional and baseline activation of AXL, Eq. 8 was used:

$$[pAkt] = \frac{B_{\max,1} [pEGFR]}{K_{D,1} + [pEGFR]} + \frac{\xi B_{\max,2} ([pEGFR] + \beta)}{K_{D,2} + ([pEGFR] + \beta)}$$

Total receptor quantification

Total receptor amounts were measured with a bead-based ELISA (Novagen). For quantification of AXL and MER, established ELISA antibodies and standards (R&D Systems) were used. The capture antibody was conjugated to unconjugated beads (Bio-Rad) and used in a multiplexed fashion with the other targets. Linearity of the assay was validated during measurement by dilution series of both the lysates and standards.

Each cell line was seeded sparsely, and the next day was starved for 4 hours and lysed. Receptor measurements were normalized to total protein content to provide a receptor mass fraction (that is, femtogram of receptor per milligram of cell lysate). This mass fraction was used in all subsequent modeling. For receptor density calculations, a subconfluent plate of cells was trypsinized the number of cells was counted and lysed and total protein was quantified. This provided the conversion, for each cell line, from milligram of lysate to number of cells. Combined with the known mass of each receptor, a value could then be converted to number of receptors per cell. Finally, receptor density was calculated by using the surface area of a HeLa cell [1600 μm^2 , BNID 103718 (62)].

Assay selection

To determine which methods might be suitable for studying such complexes on the cell surface, we developed a simple statistical model to describe the background one might expect given particular receptor expression, a characteristic distance for a particular assay, and random distribution of receptors on the surface of a cell. The background of an assay that gives signal when two receptors are within a particular distance has a background of one minus the probability of colocalization occurring by chance, given by a Poisson distribution:

$$B = 1 - p(0|\lambda) = 1 - e^{-\lambda}$$

The average number of receptors at a density of n found within a characteristic distance of R is given as:

$$\lambda = n\pi R^2$$

Integrating these, the background B of an assay with a characteristic distance of R and with a mean receptor density of n is:

$$B = 1 - e^{-n\pi R^2}$$

and for a given amount of acceptable background, the maximal characteristic radius is:

$$R = \sqrt{\frac{-\ln(1 - B)}{n\pi}}$$

Cross-linking distance modeling

T_{ij} is the amount of receptor i in cell line j . β_j encompasses variation in the efficiency of cross-linking and protein loading from experiment to experiment. α_i encompasses variation in the efficiency of antibodies for each receptor, and the amount of cross-linking between AXL and receptor i . Therefore, the amount of cross-linking X_{ij} from AXL to receptor i within experiment and cell line j is modeled as:

$$X_{ij} = \alpha_i \beta_j T_{ij} \quad i \in [1, 7], j \in [1, 4]$$

The likelihood of each observation was calculated using the distance between the amount of cross-linking predicted by a particular model and that observed as well as the SE for each measurement (all cross-linking measurements were performed with four to six technical replicates).

Constrained optimization was performed with $\alpha_i \in [0, 1]$ and $\beta_j \in [0, 1]$ using *fmincon* within MatLab. To assess confidence in robust cross-linking, individual α_i parameters were constrained as 0, and optimization was again performed. The difference in likelihood was used for assessment of cross-linking. For the globally optimal solution, initial parameters were randomly assigned repeatedly to avoid local minima. For constrained solutions, the global optimum without constraint was used as the initial parameter state.

Receptor cross-linking immunoprecipitation

Three confluent 15-cm plates of MDA-MB-231 cells were cross-linked with 1 mM EGS for 30 min at 4°C and then lysed. The lysate was clarified by centrifugation at 16,100g for 15 min, and then precleared for 30 min with agarose resin. Lysate was then incubated with protein A/G agarose and either an immunoglobulin G control, AXL, or IGF1R antibody overnight at 4°C. The next day, the resin was washed six times with lysis buffer and then incubated with 2 M hydroxylamine HCl in phosphate-buffered saline (pH 8.5) for 6 hours at 37°C. The resin was then removed and the supernatant was run on a reducing gel.

Fluorescence-activated cell sorting analysis

Cells were treated with 2 μ M R428 in full-serum medium. Twenty-four hours later, cells were trypsinized, stained, and immediately analyzed by flow cytometry. Dual staining was performed with mab225 and AF154 (R&D Systems) for 1 hour on ice. Staining for each receptor was performed separately when in conjunction with live/dead analysis. YO-PRO-1 and propidium iodide were used according to the manufacturer's guidelines (Invitrogen).

Supplementary Material

Refer to Web version on PubMed Central for supplementary material.

Acknowledgments

We thank M. Lee and S. Hughes for helpful advice throughout this study.

Funding: This work was supported by the Congressionally Directed Medical Research Programs Department of Defense Breast Cancer Research Program (W81XWH-11-1-0088 to A.S.M.), the NSF (Graduate Research Fellowship to A.S.M.), the Repligen Fellowship in Cancer Research (to A.S.M.), the Integrated Cancer Biology Program (1-U54-CA112967 to D.A.L. and F.B.G.), the Koch Institute Frontier Research Program Initiator Award, and the NIH (R01-CA96504 to D.A.L.).

REFERENCES AND NOTES

1. Yarden Y, Pines G. The ERBB network: At last cancer therapy meets systems biology. *Nat. Rev. Cancer*. 2012; 12:553–563. [PubMed: 22785351]
2. Hynes N, Lane H. ERBB receptors and cancer: The complexity of targeted inhibitors. *Nat. Rev. Cancer*. 2005; 5:341–354. [PubMed: 15864276]
3. Wilson TR, Fridlyand J, Yan Y, Penuel E, Burton L, Chan E, Peng J, Lin E, Wang Y, Sosman J, Ribas A, Li J, Moffat J, Sutherlin DP, Koeppen H, Merchant M, Neve R, Settleman J. Widespread potential for growth-factor-driven resistance to anticancer kinase inhibitors. *Nature*. 2012; 487:505–509. [PubMed: 22763448]
4. Harbinski F, Craig VJ, Sanghavi S, Jeffery D, Liu L, Sheppard KA, Wagner S, Stamm C, Bunes A, Chatenay-Rivauday C, Yao Y, He F, Lu CX, Guagnano V, Metz T, Finan PM, Hofmann F, Sellers WR, Porter JA, Myer VE, Graus-Porta D, Wilson CJ, Buckler A, Tiedt R. Rescue screens with secreted proteins reveal compensatory potential of receptor tyrosine kinases in driving cancer growth. *Cancer Discov*. 2012; 2:948–959. [PubMed: 22874768]
5. Ercan D, Zejnullahu K, Yonesaka K, Xiao Y, Capelletti M, Rogers A, Lifshits E, Brown A, Lee C, Christensen JG, Kwiatkowski DJ, Engelman JA, Janne PA. Amplification of EGFR T790M causes resistance to an irreversible EGFR inhibitor. *Oncogene*. 2010; 29:2346–2356. [PubMed: 20118985]
6. Tannock IF, Lee CM, Tunggal JK, Cowan DSM, Egorin MJ. Limited penetration of anticancer drugs through tumor tissue: A potential cause of resistance of solid tumors to chemotherapy. *Clin. Cancer Res*. 2002; 8:878–884. [PubMed: 11895922]
7. Thiery J, Acloque H, Huang R, Nieto M. Epithelial-mesenchymal transitions in development and disease. *Cell*. 2009; 139:871–890. [PubMed: 19945376]
8. Taube JH, Herschkowitz JI, Komurov K, Zhou AY, Gupta S, Yang J, Hartwell K, Onder TT, Gupta PB, Evans KW, Hollier BG, Ram PT, Lander ES, Rosen JM, Weinberg RA, Mani SA. Core epithelial-to-mesenchymal transition inter-actome gene-expression signature is associated with claudin-low metaplastic breast cancer subtypes. *Proc. Natl. Acad. Sci. U.S.A.* 2010; 107:15449–15454. [PubMed: 20713713]
9. Frederick BA, Helfrich BA, Coldren CD, Zheng D, Chan D, Bunn PA, Raben D. Epithelial to mesenchymal transition predicts gefitinib resistance in cell lines of head neck squamous cell carcinoma and non-small cell lung carcinoma. *Mol. Cancer Ther*. 2007; 6:1683–1691. [PubMed: 17541031]
10. Byers LA, Diao L, Wang J, Saintigny P, Girard L, Peyton M, Shen L, Fan YH, Giri U, Tumula P, Nilsson MB, Gudikote J, Tran HT, Cardnell RJ, Bearss DJ, Warner SL, Foulks JM, Kanner SB, Gandhi V, Krett NL, Rosen ST, Kim ES, Herbst RS, Blumenschein GR, Lee JJ, Lippman SM, Ang KK, Mills GB, Hong WK, Weinstein JN, Wistuba II, Coombes K, Minna JD, Heymach JV. An epithelial-mesenchymal transition gene signature predicts resistance to EGFR PI3K inhibitors and identifies Axl as a therapeutic target for overcoming EGFR inhibitor resistance. *Clin. Cancer Res*. 2012; 19:279–290. [PubMed: 23091115]
11. Thomson S, Petti F, Sujka-Kwok I, Epstein D, Haley JD. Kinase switching in mesenchymal-like non-small cell lung cancer lines contributes to EGFR inhibitor resistance through pathway redundancy. *Clin. Exp. Metastasis*. 2008; 25:843–854. [PubMed: 18696232]
12. Arumugam T, Ramachandran V, Fournier KF, Wang H, Marquis L, Abbruzzese JL, Gallick GE, Logsdon CD, McConkey DJ, Choi W. Epithelial to mesenchymal transition contributes to drug resistance in pancreatic cancer. *Cancer Res*. 2009; 69:5820–5828. [PubMed: 19584296]
13. Aktas B, Tewes M, Fehm T, Hauch S, Kimmig R, Kasimir-Bauer S. Stem cell and epithelial-mesenchymal transition markers are frequently overexpressed in circulating tumor cells of metastatic breast cancer patients. *Breast Cancer Res*. 2009; 11:R46. [PubMed: 19589136]
14. Creighton CJ, Li X, Landis M, Dixon JM, Neumeister VM, Sjolund A, Rimm DL, Wong H, Rodriguez A, Herschkowitz JI, Fan C, Zhang X, He X, Pavlick A, Gutierrez MC, Renshaw L, Larionov AA, Faratian D, Hilsenbeck SG, Perou CM, Lewis MT, Rosen JM, Chang JC. Residual breast cancers after conventional therapy display mesenchymal as well as tumor-initiating features. *Proc. Natl. Acad. Sci. U.S.A.* 2009; 106:13820–13825. [PubMed: 19666588]

15. Li QQ, Xu JD, Wang WJ, Cao XX, Chen Q, Tang F, Chen ZQ, Liu XP, Xu ZD. Twist1-mediated Adriamycin-induced epithelial-mesenchymal transition relates to multidrug resistance invasive potential in breast cancer cells. *Clin. Cancer Res.* 2009; 15:2657–2665. [PubMed: 19336515]
16. Thomson S, Petti F, Sujka-Kwok I, Mercado P, Bean J, Monaghan M, Seymour SL, Argast GM, Epstein DM, Haley JD. A systems view of epithelial-mesenchymal transition signaling states. *Clin. Exp. Metastasis.* 2011; 28:137–155. [PubMed: 21194007]
17. Shapiro IM, Cheng AW, Flytzanis NC, Balsamo M, Condeelis JS, Oktay MH, Burge CB, Gertler FB. An EMT-driven alternative splicing program occurs in human breast cancer and modulates cellular phenotype. *PLoS Genet.* 2011; 7:e1002218. [PubMed: 21876675]
18. Lapuk A, Marr H, Jakkula L, Pedro H, Bhattacharya S, Purdom E, Hu Z, Simpson K, Pachter L, Durinck S, Wang N, Parvin B, Fontenay G, Speed T, Garbe J, Stampfer M, Bayandorian H, Dorton S, Clark TA, Schweitzer A, Wyrobek A, Feiler H, Spellman P, Conboy J, Gray JW. Exon-level microarray analyses identify alternative splicing programs in breast cancer. *Mol. Cancer Res.* 2010; 8:961–974. [PubMed: 20605923]
19. Kim HD, Meyer AS, Wagner JP, Alford SK, Wells A, Gertler FB, Lauffenburger DA. Signaling network state predicts twist-mediated effects on breast cell migration across diverse growth factor contexts. *Mol. Cell. Proteomics.* 2011; 10 M111.008433.
20. Craven RJ, Xu LH, Weiner TM, Fridell YW, Dent GA, Srivastava S, Varnum B, Liu ET, Cance WG. Receptor tyrosine kinases expressed in metastatic colon cancer. *Int. J. Cancer.* 1995; 60:791–797. [PubMed: 7896447]
21. Nemoto T, Ohashi K, Akashi T, Johnson JD, Hirokawa K. Overexpression of protein tyrosine kinases in human esophageal cancer. *Pathobiology.* 1997; 65:195–203. [PubMed: 9396043]
22. Ito M, Nakashima M, Nakayama T, Ohtsuru A, Nagayama Y, Takamura N, Demedchik EP, Sekine I, Yamashita S. Expression of receptor-type tyrosine AXL kinase its ligand Gas6 in pediatric thyroid carcinomas around Chernobyl. *Thyroid.* 2002; 12:971–975. [PubMed: 12490074]
23. Berclaz G, Altermatt HJ, Rohrbach V, Kieffer I, Dreher E, Andres AC. Estrogen dependent expression of the receptor tyrosine kinase AXL in normal malignant human breast. *Ann. Oncol.* 2001; 12:819–824. [PubMed: 11484958]
24. Shieh YS, Lai CY, Kao YR, Shiah SG, Chu YW, Lee HS, Wu CW. Expression of Axl in lung adenocarcinoma and correlation with tumor progression. *Neoplasia.* 2005; 7:1058–1064. [PubMed: 16354588]
25. Hutterer M, Knyazev P, Abate A, Reschke M, Maier H, Stefanova N, Knyazeva T, Barbieri V, Reindl M, Muigg A, Kostron H, Stockhammer G, Ullrich A. Axl growth arrest-specific gene 6 are frequently overexpressed in human gliomas and predict poor prognosis in patients with glioblastoma multiforme. *Clin. Cancer Res.* 2008; 14:130–138. [PubMed: 18172262]
26. Green J, Ikram M, Vyas J, Patel N, Proby CM, Ghali L, Leigh IM, O'Toole EA, Storey A. Overexpression of the Axl tyrosine kinase receptor in cutaneous SCC-derived cell lines and tumours. *Br. J. Cancer.* 2006; 94:1446–1451. [PubMed: 16641895]
27. Koorstra JBM, Karikari CA, Feldmann G, Bisht S, Rojas PL, Offerhaus GJA, Alvarez H, Maitra A. The Axl receptor tyrosine kinase confers an adverse prognostic influence in pancreatic cancer represents new therapeutic target. *Cancer Biol. Ther.* 2009; 8:618–626. [PubMed: 19252414]
28. Gjerdrum C, Tiron C, Høiby T, Stefansson I, Haugen H, Sandal T, Collett K, Li S, McCormack E, Gjertsen B, Micklem DR, Akslen LA, Glackin C, Lorens JB. Axl is an essential epithelial-to-mesenchymal transition-induced regulator of breast cancer metastasis patient survival. *Proc. Natl. Acad. Sci. U.S.A.* 2010; 107:1124–1129. [PubMed: 20080645]
29. Johannessen CM, Boehm JS, Kim SY, Thomas SR, Wardwell L, Johnson LA, Emery CM, Stransky N, Cogdill AP, Barretina J, Caponigro G, Hieronymus H, Murray RR, Salehi-Ashtiani K, Hill DE, Vidal M, Zhao JJ, Yang X, Alkan O, Kim S, Harris JL, Wilson CJ, Myer VE, Finan PM, Root DE, Roberts TM, Golub T, Flaherty KT, Dummer R, Weber BL, Sellers WR, Schlegel R, Wargo JA, Hahn WC, Garraway LA. COT drives resistance to RAF inhibition through MAP kinase pathway reactivation. *Nature.* 2010; 468:968–972. [PubMed: 21107320]
30. Liu L, Greger J, Shi H, Liu Y, Greshock J, Annan R, Halsey W, Sathe GM, Martin AM, Gilmer TM. Novel mechanism of lapatinib resistance in HER2-positive breast tumor cells: Activation of AXL. *Cancer Res.* 2009; 69:6871–6878. [PubMed: 19671800]

31. Shiozawa Y, Pedersen EA, Patel LR, Ziegler AM, Havens AM, Jung Y, Wang J, Zalucha S, Loberg RD, Pienta KJ, Taichman RS. Gas6/AXL axis regulates prostate cancer invasion proliferation and survival in the bone marrow niche. *Neoplasia*. 2010; 12:116–127. [PubMed: 20126470]
32. Vuoriluoto K, Haugen H, Kiviluoto S, Mpindi JP, Nevo J, Gjerdrum C, Tiron C, Lorens JB, Ivaska J. Vimentin regulates EMT induction by Slug and oncogenic H-Ras and migration by governing Axl expression in breast cancer. *Oncogene*. 2011; 30:1436–1448. [PubMed: 21057535]
33. Zhang Z, Lee JC, Lin L, Olivas V, Au V, LaFramboise T, Abdel-Rahman M, Wang X, Levine AD, Rho JK, Choi YJ, Choi C-M, Kim S-W, Jang SJ, Park YS, Kim WS, Lee DH, Lee J-S, Miller VA, Arcila M, Ladanyi M, Moonsamy P, Sawyers C, Boggon TJ, Ma PC, Costa C, Taron M, Rosell R, Halmos B, Bivona TG. Activation of the AXL kinase causes resistance to EGFR-targeted therapy in lung cancer. *Nat. Genet.* 2012; 44:852–860. [PubMed: 22751098]
34. Tai KY, Shieh YS, Lee CS, Shiah SG, Wu CW. Axl promotes cell invasion by inducing MMP-9 activity through activation of NF- κ B and Brg-1. *Oncogene*. 2008; 27:4044–4055. [PubMed: 18345028]
35. McCloskey P, Pierce J, Koski RA, Varnum B, Liu ET. Activation of the Axl receptor tyrosine kinase induces mitogenesis and transformation in 32D cells. *Cell Growth Differ.* 1994; 5:1105–1117. [PubMed: 7848912]
36. Hafizi S, Alindri F, Karlsson R, Dahlbäck B. Interaction of Axl receptor tyrosine kinase with C1-TEN a novel C1 domain-containing protein with homology to tensin. *Biochem. Biophys. Res. Commun.* 2002; 299:793–800. [PubMed: 12470648]
37. Huang PH, Mukasa A, Bonavia R, Flynn RA, Brewer ZE, Cavenee WK, Furnari FB, White FM. Quantitative analysis of EGFRvIII cellular signaling networks reveals a combinatorial therapeutic strategy for glioblastoma. *Proc. Natl. Acad. Sci. U.S.A.* 2007; 104:12867–12872. [PubMed: 17646646]
38. Barretina J, Caponigro G, Stransky N, Venkatesan K, Margolin AA, Kim S, Wilson CJ, Lehár J, Kryukov GV, Sonkin D, Reddy A, Liu M, Murray L, Berger MF, Monahan JE, Morais P, Meltzer J, Korejwa A, Jané-Valbuena J, Mapa FA, Thibault J, Bric-Furlong E, Raman P, Shipway A, Engels IH, Cheng J, Yu GK, Yu J, Aspesi P, de Silva M, Jagtap K, Jones MD, Wang L, Hatton C, Palescandolo E, Gupta S, Mahan S, Sougnez C, Onofrio RC, Liefeld T, MacConaill L, Winckler W, Reich M, Li N, Mesirov JP, Gabriel SB, Getz G, Ardlie K, Chan V, Myer VE, Weber BL, Porter J, Warmuth M, Finan P, Harris JL, Meyerson M, Golub TR, Morrissey MP, Sellers WR, Schlegel R, Garraway LA. The Cancer Cell Line Encyclopedia enables predictive modelling of anticancer drug sensitivity. *Nature*. 2012; 483:603–607. [PubMed: 22460905]
39. Bishop, CM. *Pattern Recognition and Machine Learning*. New York: Springer; 2006.
40. Cancer Genome Atlas Network. Comprehensive molecular portraits of human breast tumours. *Nature*. 2012; 490:61–70. [PubMed: 23000897]
41. Zhuang G, Brantley-Sieders DM, Vaught D, Yu J, Xie L, Wells S, Jackson D, Muraoka-Cook R, Arteaga C, Chen J. Elevation of receptor tyrosine kinase EphA2 mediates resistance to trastuzumab therapy. *Cancer Res.* 2010; 70:299–308. [PubMed: 20028874]
42. Lee MJ, Ye AS, Gardino AK, Heijink AM, Sorger PK, MacBeath G, Yaffe MB. Sequential application of anticancer drugs enhances cell death by rewiring apoptotic signaling networks. *Cell*. 2012; 149:780–794. [PubMed: 22579283]
43. Nagane M, Levitzki A, Gazit A, Cavenee WK, Huang HJ. Drug resistance of human glioblastoma cells conferred by a tumor-specific mutant epidermal growth factor receptor through modulation of Bcl-X_L and caspase-3-like proteases. *Proc. Natl. Acad. Sci. U.S.A.* 1998; 95:5724–5729. [PubMed: 9576951]
44. Li Y, Ye X, Tan C, Hongo JA, Zha J, Liu J, Kallop D, Ludlam MJC, Pei L. Axl as a potential therapeutic target in cancer: Role of Axl in tumor growth metastasis and angiogenesis. *Oncogene*. 2009; 28:3442–3455. [PubMed: 19633687]
45. Mark MR, Chen J, Hammonds RG, Sadick M, Godowsk PJ. Characterization of Gas6 a member of the superfamily of G domain-containing proteins as a ligand for Rse Axl. *J. Biol. Chem.* 1996; 271:9785–9789. [PubMed: 8621659]
46. Hasanbasic I, Rajotte I, Blostein M. The role of γ -carboxylation in the anti-apoptotic function of gas6. *J. Thromb. Haemost.* 2005; 3:2790–2797. [PubMed: 16359517]

47. Meyer AS, Hughes-Alford SK, Kay JE, Castillo A, Wells A, Gertler FB, Lauffenburger DA. 2D protrusion but not motility predicts growth factor-induced cancer cell migration in 3D collagen. *J. Cell Biol.* 2012; 197:721–729. [PubMed: 22665521]
48. Gusenbauer S, Vlaicu P, Ullrich A. HGF induces novel EGFR functions involved in resistance formation to tyrosine kinase inhibitors. *Oncogene.* 2012;2012
49. Roussos ET, Balsamo M, Alford SK, Wyckoff JB, Gligorijevic B, Wang Y, Pozzuto M, Stobezki R, Goswami S, Segall JE, Lauffenburger DA, Bresnick AR, Gertler FB, Condeelis JS. Mena invasive (Mena^{INV}) promotes multicellular streaming motility transendothelial migration in a mouse model of breast cancer. *J. Cell Sci.* 2011; 124:2120–2131. [PubMed: 21670198]
50. Cerchia L, Esposito CL, Camorani S, Rienzo A, Stasio L, Insabato L, Affuso A, de Franciscis V. Targeting Axl with an high-affinity inhibitory aptamer. *Mol. Ther.* 2012; 20:2291–2303. [PubMed: 22910292]
51. Ye X, Li Y, Stawicki S, Couto S, Eastham-Anderson J, Kallop D, Weimer R, Wu Y, Pei L. An anti-Axl monoclonal antibody attenuates xenograft tumor growth and enhances the effect of multiple anticancer therapies. *Oncogene.* 2010; 29:5254–5264. [PubMed: 20603615]
52. Martens T, Schmidt NO, Eckerich C, Fillbrandt R, Merchant M, Schwall R, Westphal M, Lamszus K. A novel one-armed anti-c-Met antibody inhibits glioblastoma growth in vivo. *Clin. Cancer Res.* 2006; 12:6144–6152. [PubMed: 17062691]
53. Jin H, Yang R, Zheng Z, Romero M, Ross J, Bou-Reslan H, Carano RAD, Kasman I, Mai E, Young J, Zha J, Zhang Z, Ross S, Schwall R, Colbern G, Merchant M. MetMab, the one-armed 5D5 anti-c-Met antibody, inhibits orthotopic pancreatic tumor growth and improves survival. *Cancer Res.* 2008; 68:4360–4368. [PubMed: 18519697]
54. Holland S, Pan A, Franci C, Hu Y, Chang B, Li W, Duan M, Torneros A, Yu J, Heckrodt TJ, Zhang J, Ding P, Apatira A, Chua J, Brandt R, Pine P, Goff D, Singh R, Payan DG, Hitoshi Y. R428, a selective small molecule inhibitor of Axl kinase, blocks tumor spread and prolongs survival in models of metastatic breast cancer. *Cancer Res.* 2010; 4:1544–1554. [PubMed: 20145120]
55. Riely GJ, Kris MG, Zhao B, Akhurst T, Milton DT, Moore E, Tyson L, Pao W, Rizvi NA, Schwartz LH, Miller VA. Prospective assessment of discontinuation reinitiation of erlotinib or gefitinib in patients with acquired resistance to erlotinib or gefitinib followed by the addition of everolimus. *Clin. Cancer Res.* 2007; 13:5150–5155. [PubMed: 17785570]
56. Chaft JE, Oxnard GR, Sima CS, Kris MG, Miller VA, Riely GJ. Disease flare after tyrosine kinase inhibitor discontinuation in patients with EGFR-mutant lung cancer acquired resistance to erlotinib or gefitinib: Implications for clinical trial design. *Clin. Cancer Res.* 2011; 17:6298–6303. [PubMed: 21856766]
57. Pop O, Pirvu A, Toffart AC, Moro-Sibilot D. Disease flare after treatment discontinuation in a patient with EML4-ALK lung cancer acquired resistance to crizotinib. *J. Thorac. Oncol.* 2012; 7:e1–e2. [PubMed: 22797152]
58. Yeh CY, Shin SM, Yeh HH, Wu TJ, Shin JW, Chang TY, Raghavaraju G, Lee CT, Chiang JH, Tseng VS, Lee YCG, Shen CH, Chow NH, Liu HS. Transcriptional activation of the Axl and PDGFR- α by c-Met through a ras- and Src-independent mechanism in human bladder cancer. *BMC Cancer.* 2011; 11:139. [PubMed: 21496277]
59. Greco WR, Bravo G, Parsons JC. The search for synergy: A critical review from a response surface perspective. *Pharmacol. Rev.* 1995; 47:331–385. [PubMed: 7568331]
60. Efron B, Gong G. A leisurely look at the bootstrap the jackknife, and cross-validation. *Am. Stat.* 1983; 37:36–48.
61. Hurvich CM, Tsai CL. Bias of the corrected AIC criterion for underfitted regression and time series models. *Biometrika.* 1991; 78:499–509.
62. Milo R, Jorgensen P, Moran U, Weber G, Springer M. BioNumbers—The database of key numbers in molecular and cell biology. *Nucleic Acids Res.* 2010; 38:D750–D753. [PubMed: 19854939]

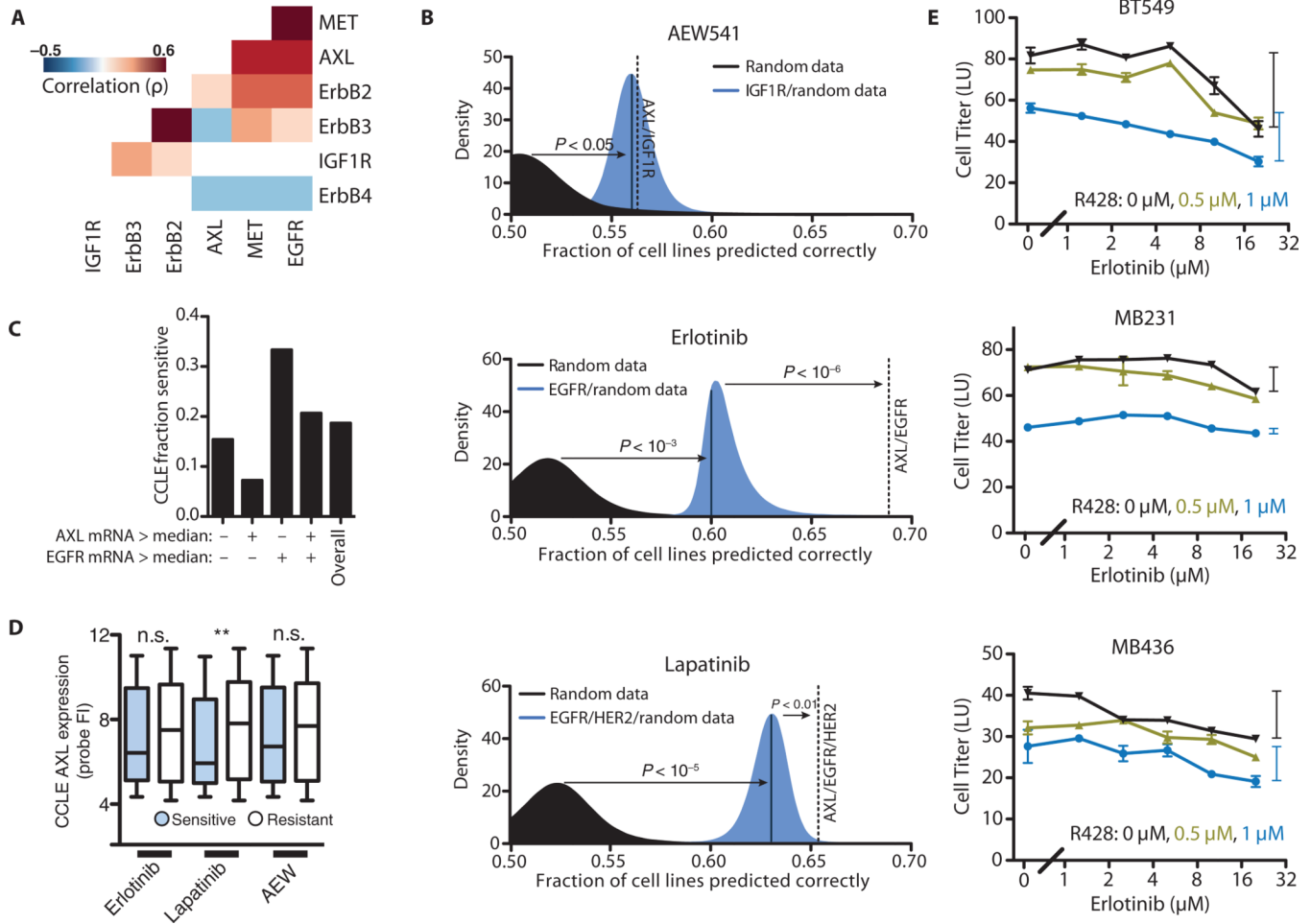


Fig. 1. Support vector classification to identify mechanisms of drug resistance
(A) Spearman correlations of expression for a subset of RTKs. Only statistically significant correlations are shown ($P < 0.01$). **(B)** Classification of cell lines as resistant or sensitive to AEW541, erlotinib, and lapatinib based on RTK expression. Classification accuracy using randomized expression data (black), a model considering the expression of the gene encoding the drug target receptor (blue), or a model considering the expression of both the gene encoding the drug target receptor and that of *AXL* (dotted line) are shown. **(C)** Fraction of cell lines that are sensitive to erlotinib after separation according to those that exhibit greater or less than median expression of *EGFR* or *AXL*. **(D)** *AXL* expression probe values for resistant and sensitive cell lines to each drug (** $P < 0.01$, Kruskal-Wallis test, $n = 91$ to 396 cell lines per grouping). FI, fluorescence intensity; n.s., not significant. **(E)** Dose-response curves for R428 and erlotinib in three TNBC cell lines that have abundant *EGFR* and *AXL*. Bars on the side indicate the range of viability between the highest and lowest erlotinib dose to illustrate subadditivity ($P < 10^{-6}$, BT549; $P < 0.05$, MB436; $P < 0.01$, MB231 by Loewe's synergy analysis; see Materials and Methods) between erlotinib and R428. Data are means \pm SEM from three independent biological measurements.

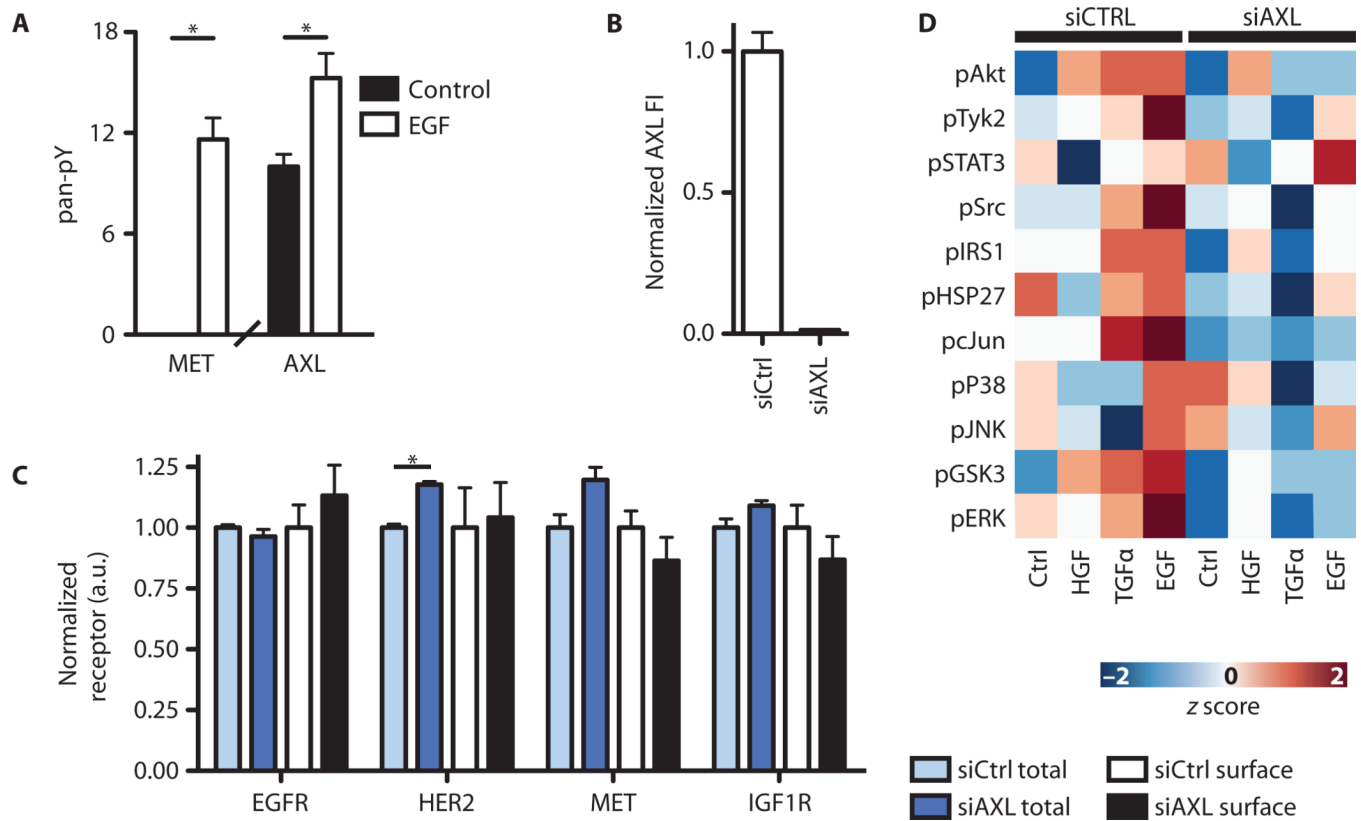


Fig. 2. EGF stimulation transactivates AXL and MET

(A) ELISA-based pan-phosphotyrosine (pan-pY) measurement of alternative receptors after EGF stimulation in MDA-MB-231 (* $P < 0.05$, Student's t test). (B) AXL knockdown, measured by ELISA. (C) Total and surface amounts of alternative receptors in AXL-silenced MDA-MB-231 cells (* $P < 0.05$, Student's t test). Data are means \pm SEM of three biological measurements. (D) Downstream signaling assessed by kinase phosphorylation in MDA-MB-231 cells 5 min after stimulation with EGF, TGFA, or HGF in the presence or absence (siAXL) of AXL. Each phosphosite was mean-centered and variance-normalized.

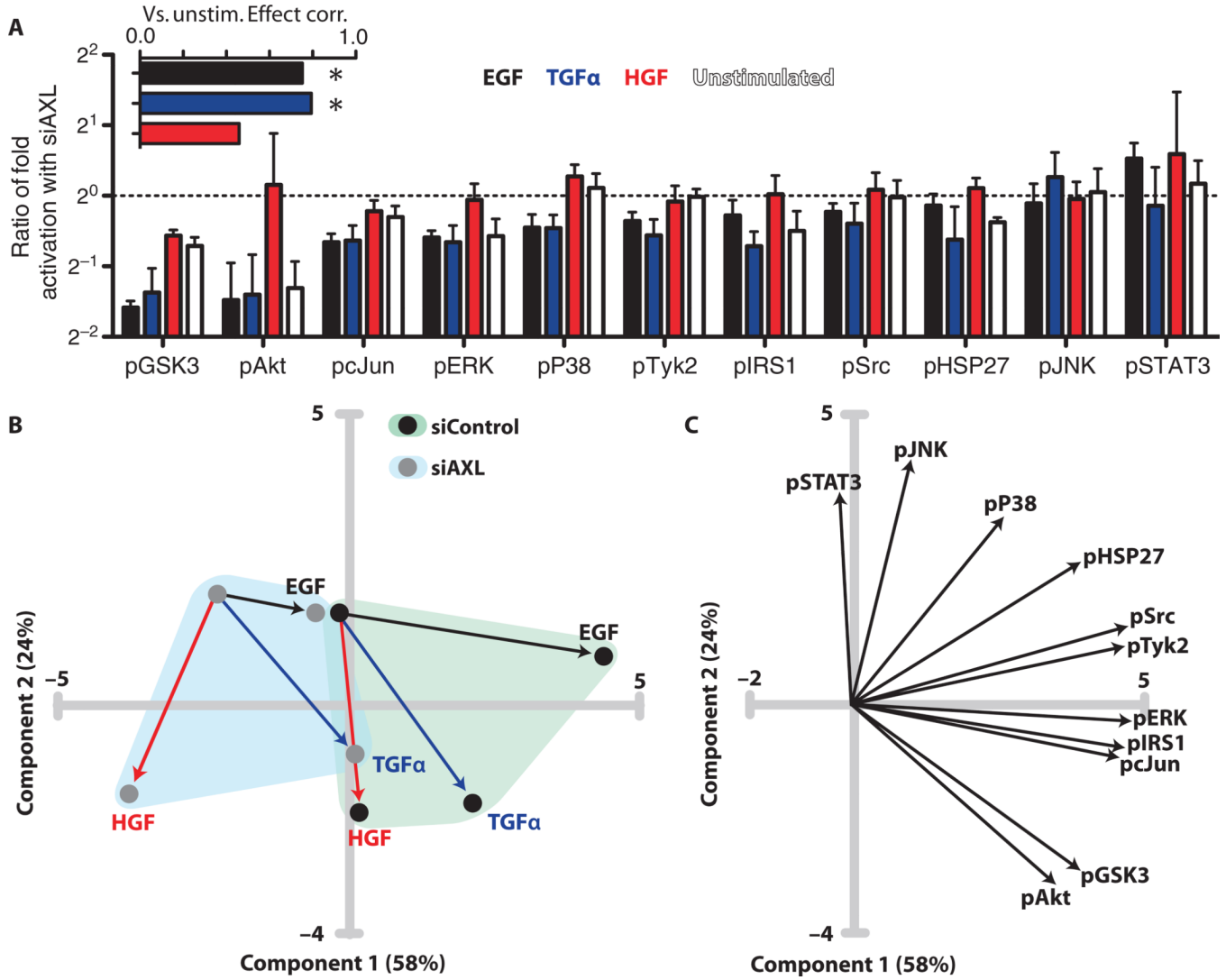


Fig. 3. AXL knockdown attenuates downstream signaling in MDA-MB-231

(A) Ratios of fold activation after treatment with growth factor in AXL knockdown cells relative to wild-type cells: $([siAXL\ GF]/[siAXL\ Unstim]) \div ([siControl\ GF]/[siControl\ Unstim])$. The unstimulated bar indicates the ratio of unstimulated abundance: $[siAXL\ Unstim]/[siControl\ Unstim]$. Inset shows the Spearman correlation across all phosphosites between the unstimulated and stimulated ratios ($*P < 0.05$). (B) PCA score plot of signaling data after AXL knockdown. Line colors indicate stimulation conditions denoted in (A). (C) Loading plot of signaling data after AXL knockdown.

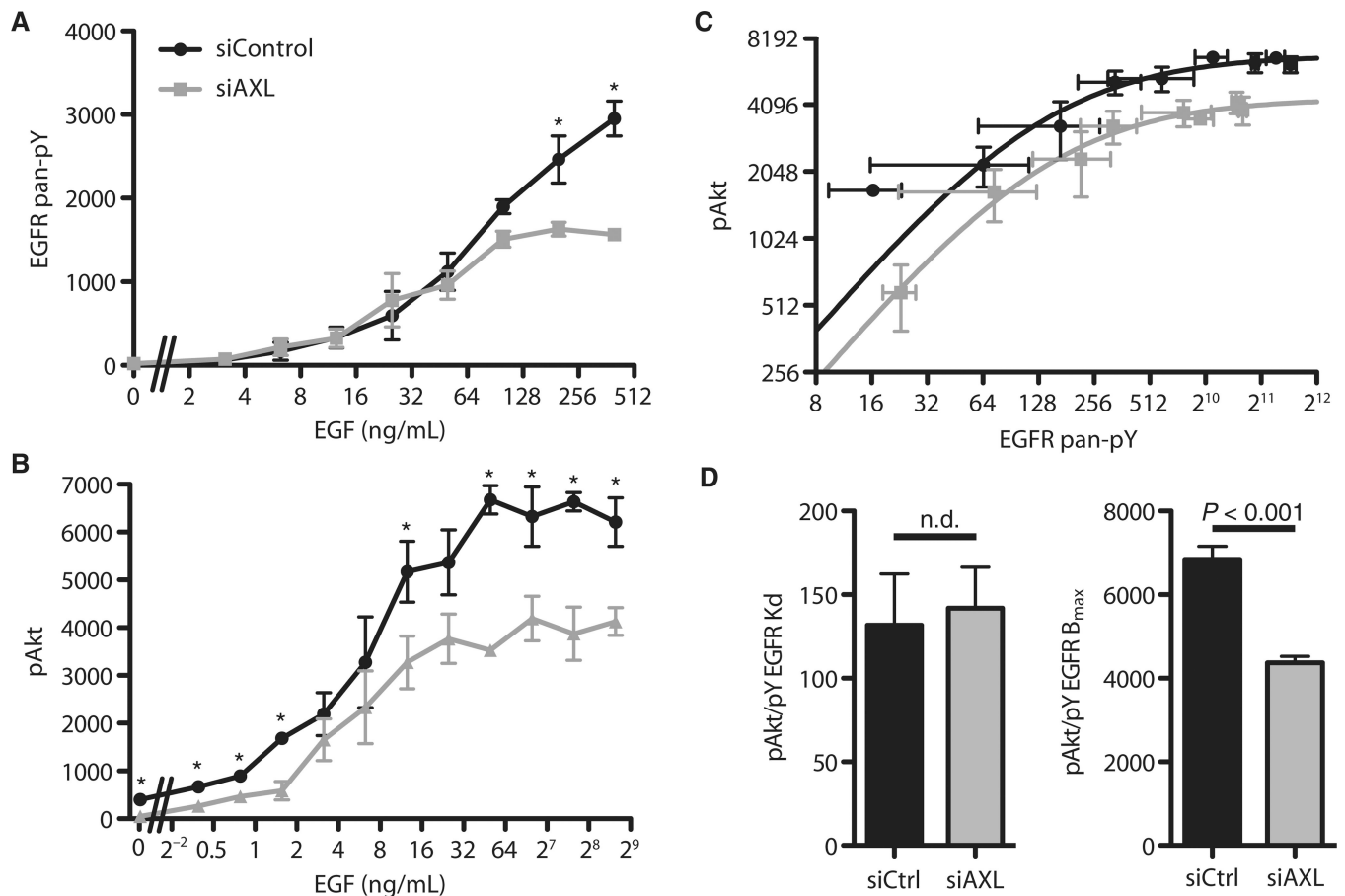


Fig. 4. AXL amplifies the EGFR signaling response

(A) ELISA of pan-pY EGFR in wild-type (siControl) or AXL-silenced (siAXL) MDA-MB-231 after 5 min of treatment with varying EGF amounts. Data are means \pm SEM. $P < 0.05$, Student's t test. $n = 3$. (B) Phosphorylation of Akt in response to a range of EGF doses. Data are means \pm SEM. $P < 0.05$, Student's t test. $n = 3$. (C) ELISA for the abundance of pan-pY on EGFR versus the phosphorylation of Akt in MDA-MB-231 cells. Lines show a Hill regression to each set of data with SE of biological triplicate measurements. (D) Hill regression of each plot shows similar K_d values but significantly different maximal activation (F test). Error bars indicate SE of the fit.

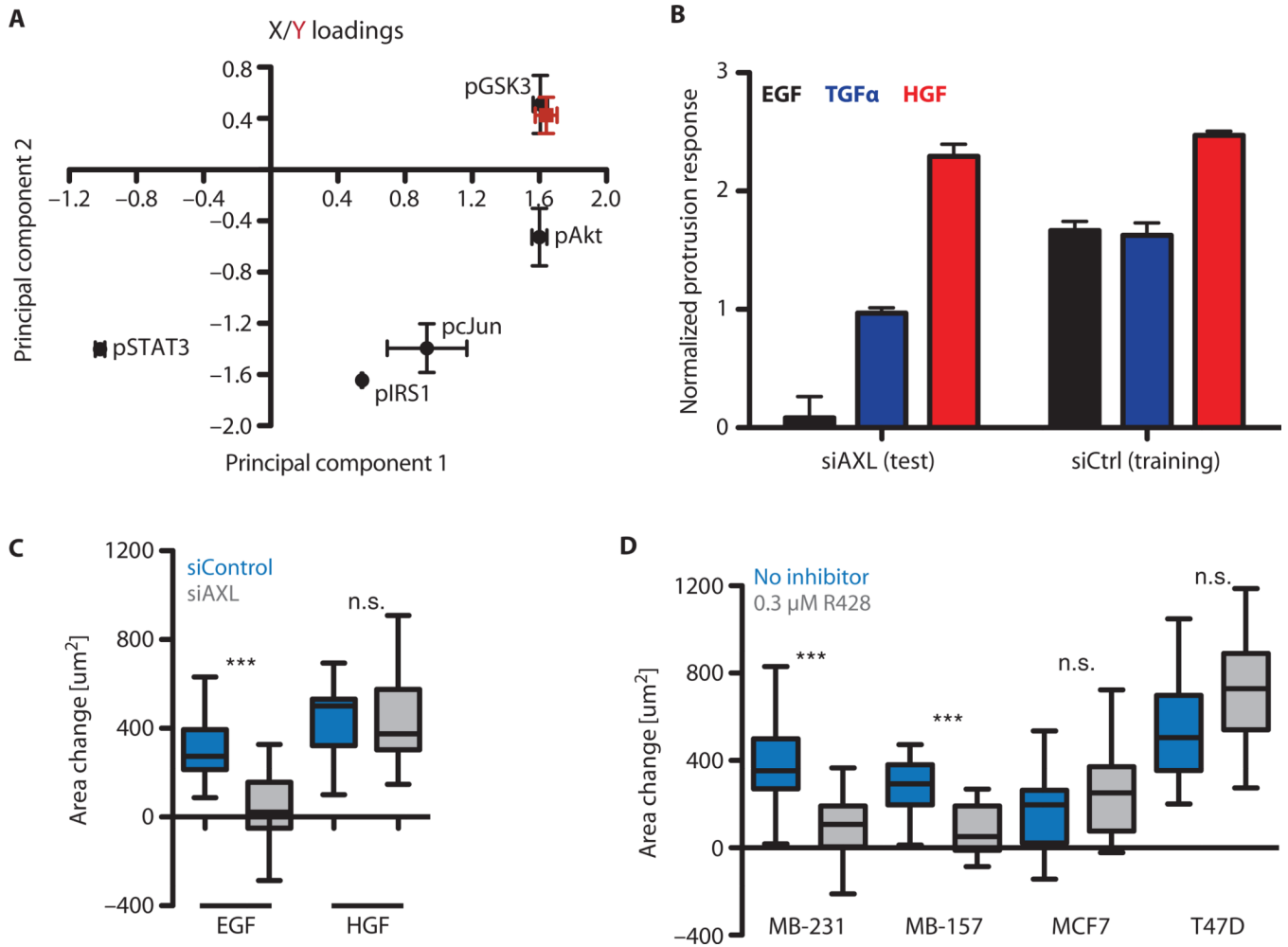


Fig. 5. AXL signaling is required for EGF-elicited protrusion

(A) Mean loadings of the reduced partial least-squares regression models. The red point corresponds to the projection of the phenotype. Error bars indicate the SE for the family of reduced models. (B) Protrusion predictions from reduced partial least-squares regression models for wild-type (by cross-validation) and AXL knockdown (by prediction) cells. Error bars indicate the SE of prediction across the family of reduced models. (C) EGF-elicited protrusion response of MDA-MB-231 cells upon AXL knockdown ($***P < 0.001$, Mann-Whitney test; $n = 13$ to 25 from three independent experiments). (D) EGF-elicited protrusion responses with or without 0.3 μM R428 ($***P < 0.001$, Mann-Whitney test; $n = 17$ to 35 from three independent experiments). MDA-MB-231 and MDA-MB-157 cells express AXL, whereas MCF7 and T47D cells do not.

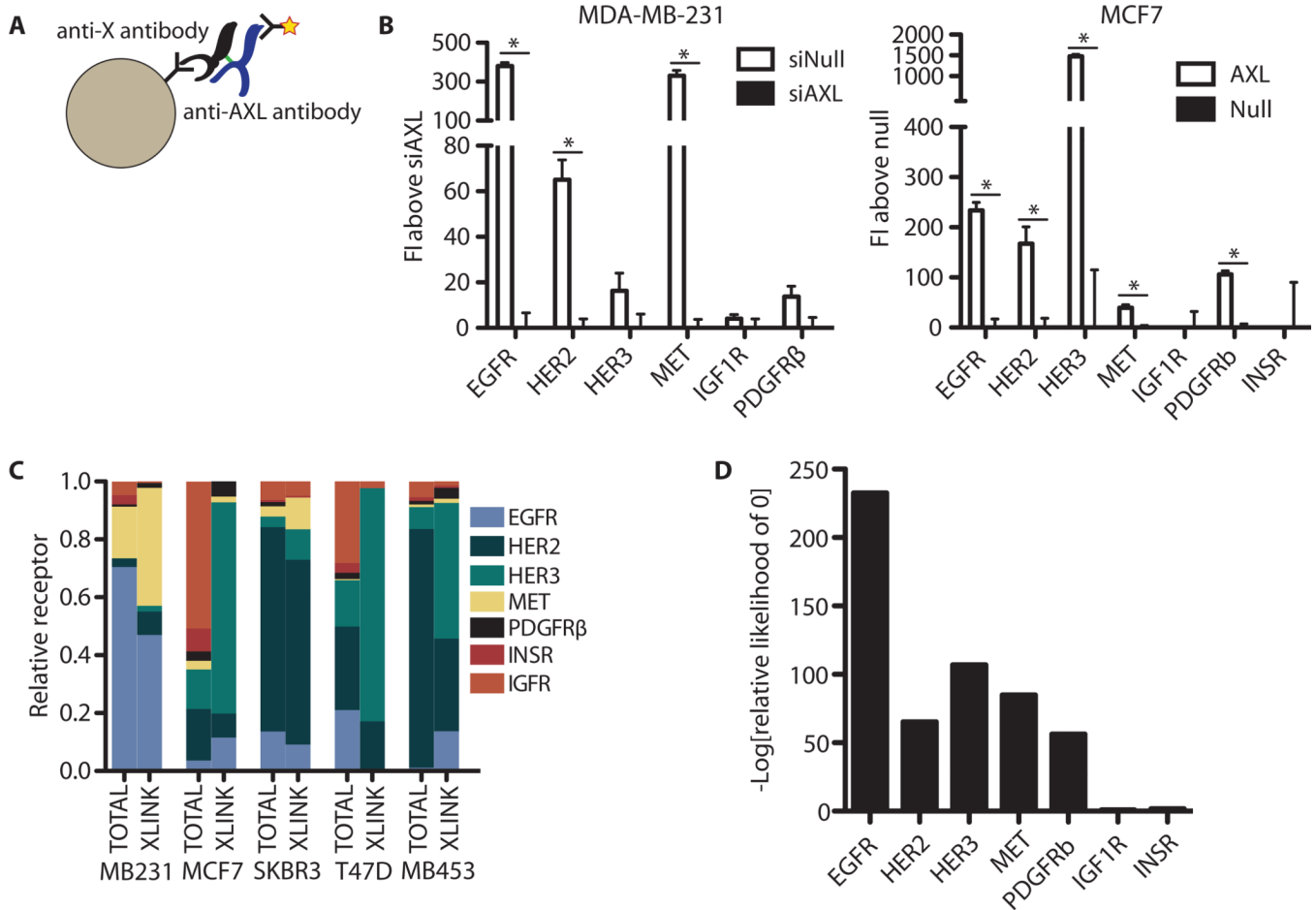


Fig. 6. AXL colocalizes with ErbB receptors and MET

(A) Illustration of the multivariate cross-linking-mediated coimmunoprecipitation procedure adopted. After ethylene glycolbis(succinimidylsuccinate) (EGS) cross-linking, cells are lysed and incubated with identifiable beads targeting non-AXL RTKs, then with an antibody for AXL to quantify the amount of receptor coimmunoprecipitation. (B) Quantification of AXL in complex with the indicated receptor in MDA-MB-231 and MCF7 cells. To account for possible antibody crosstalk, samples were always compared to those with AXL modulated by either siRNA-mediated knockdown (siAXL) or exogenous expression (AXL) in MDA-MB-231 or MCF7 cells, respectively. Data are means \pm SE FI from six technical replicates across biological duplicates; $P < 0.05$, Student's t test. (C) Summary of the relative amount of the indicated receptor found in AXL-linked complexes assessed by direct ELISA (TOTAL) or cross-receptor measurement (XLINK) from each cell line in cross-linked lysates. Data are representative of two separate experiments, each with technical triplicates. (D) Relative likelihood of each parameter being 0 (no complex occurring with AXL) for each receptor across all five cell lines.

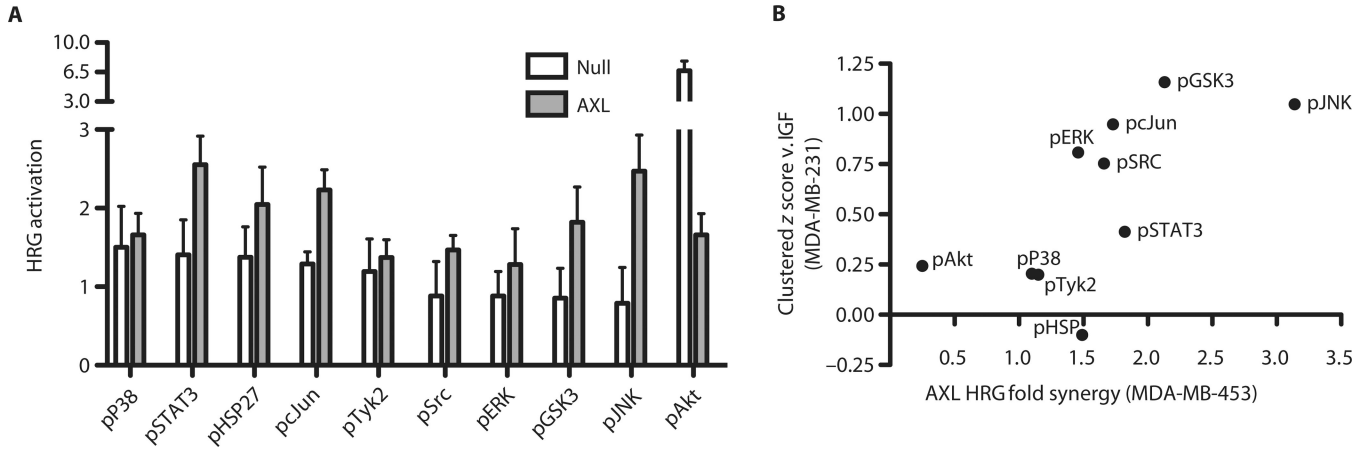


Fig. 7. Cross-linking predicts HRG-AXL crosstalk in MDA-MB-453

(A) Fold activation of downstream signaling after HRG stimulation in cells with or without exogenous AXL expression. (B) For the effect of clustered receptors in MDA-MB-231, the signaling measurement of IGF-stimulated cells was z score-normalized to the mean measurement of EGF-, TGF α -, HGF-, HRG-, and HBEGF-stimulated cells. For synergy in MDA-MB-453 cells (which do not normally express AXL), the ratio of fold activation after HRG treatment in cells overexpressing AXL to that in cells that do not express AXL is shown. $P = 0.027$, Spearman correlation.